SAND2013-10383C

In-cylinder soot precursor growth in a low-temperature combustion diesel engine: laser-induced fluorescence of polycyclic aromatic hydrocarbons

C.A.J. Leermakers

Department of Mechanical Engineering, Eindhoven University of Technology, P.O. Box 513, GEM-N 1.21, 5600 MB, Eindhoven, The Netherlands

M.P.B. Musculus*

Combustion Research Facility, Sandia National Laboratories, P.O. Box 969, MS 9053, Livermore, CA 94551, USA

*Corresponding author: Fax: +1 (925) 294-1004, e-mail: mpmuscu@sandia.gov

Colloquium: IC engine and gas turbine combustion (alternatives: Soot, PAH, and other large molecules; Diagnostics)

Word count according to **method 1**:

Introduction				**409**	
Body				**2738**	
Conclusions				**454**	
Acknowledgements				**66**	
Equations				**0**	
Nomenclature				**0**	
References	21			**402**	**4069**
Tables	lines	cols			
1	13	1		114	**114**
Figures	h (mm)	cols	caption		
1	80	1	25	223	
2	103.3	2	66	564.52	
3	63.5	2	69	392.4	
4	50.8	1	35	168.76	
5	49.5	1	33	163.9	
					1513
				5696	

The authors DO NOT agree to pay charges for color reproduction of figures. All figures to be printed in grey scale.

Abstract: The growth of poly-cyclic aromatic hydrocarbon (PAH) soot precursors are observed using a two-laser technique combining laser-induced fluorescence (LIF) of PAH with laser-induced incandescence (LII) of soot in a diesel engine under low-temperature combustion (LTC) conditions. The broad mixture distributions and slowed chemical kinetics of LTC "stretch out" soot-formation processes in both space and time, thereby facilitating their study. Imaging PAH-LIF from pulsed-laser excitation at three discrete wavelengths (266, 532, and 633 nm) reveals the temporal growth of PAH molecules, while soot-LII from a 1064-nm pulsed laser indicates inception to soot. The distribution of PAH-LIF also grows spatially within the combustion chamber before soot-LII is first detected. The PAH-LIF signals have broad spectra, much like LII, but typically with a color temperature that is far to hot for laser-heated soot. Quantitative natural-emission spectroscopy also shows a broad emission spectrum, presumably from PAH chemiluminescence, temporally coinciding with of the PAH-LIF.

Keywords: Polycyclic aromatic hydrocarbons; Particulate matter; Laser-induced fluorescence; laser-induced incandescence; Diesel low-temperature combustion

1. Introduction

Strategies to reduce pollutant emissions from diesel engines while maintaining fuel efficiency are of interest for meeting environmental regulations and market demands. Low-temperature combustion (LTC) is one in-cylinder strategy that uses dilute mixtures and enhanced premixing to maintain or even improve fuel efficiency while reducing pollutant emissions, including soot [1]. In addition to its practical utility, the broad mixture distributions and slowed chemical-kinetics of LTC conditions "stretch out" soot-formation processes in both space and time, thereby facilitating their study.

Poly-cyclic aromatic hydrocarbons (PAH) are an important class of soot precursors [2]. Smaller PAH with one to five rings may be either fuel-borne [3] or combustion-generated. Larger PAH with more than five rings are almost entirely due to combustion-induced formation and/or growth. In addition to toxicity/carcinogenicity [4], PAH formation is undesirable because they contribute to particulate matter (soot) [5].

PAH growth during combustion can be observed to some degree through spectroscopic techniques. The absorption/emission spectra of PAH molecules shift to longer wavelengths with increasing number of rings [6,7]. Individual PAH spectra are broadband and overlap with each other, however, so specific PAH species generally cannot be isolated spectrally.

One technique to probe the absorption redshift due to PAH growth is laser-induced fluorescence (LIF). If soot is present, the laser-induced emission can also include significant laser-induced incandescence (LII) of soot, which is also spectrally broad. One way to discriminate soot-LII from PAH-LIF is to use a second laser pulse at a wavelength that yields only soot-LII. The Nd:YAG laser fundamental at 1064 nm should yield only soot-LII, because even very large PAH do not display single-photon absorption at near-infrared wavelengths [8,9]. Comparisons of the two signals, acquired virtually simultaneously, thus allow discrimination of PAH-only regions from regions with both PAH and soot.

This two-laser LIF-LII approach for diesel combustion follows previous work [10], using only 532-nm PAH-LIF. Here, the PAH-LIF is extended over a broader excitation wavelength range, adding 266 and 633 nm, to study the spatio-temporal evolution of both small and very large PAH. Excitation at 266 nm probes small PAH that do not absorb at 532 nm, while the 633-nm laser may excite very large PAH that could conceivably absorb at 633 nm. Such absorption, if present, would confound soot extinction techniques that use 633-nm (i.e. HeNe) laser light [11]. Both the soot-LII and the PAH-LIF signals are also spectrally resolved to further discriminate LIF from LII, and quantitative chemiluminescence spectra provide further insight into PAH growth.

2. Experiment set-up

2.1. Optical engine and operating conditions

The optical engine is a single-cylinder Bowditch-piston version of a Cummins N14 heavy-duty diesel (bore 139.7 mm, stroke 152.4 mm, 2.34 L). Table 1 shows operating conditions and some engine specifications (see [12,13] for more engine details).

In the experiment schematic of Fig. 1, a flat fused-silica piston-crown window provides imaging access from below to the open, right-cylindrical bowl (diameter 97.8 mm). A 30-mm-wide curved window matching the piston bowl-wall contour and a flat rectangular cylinder-wall window provide laser access into the piston bowl, even near top-dead center.

A target load of 6 bar gross indicated mean-effective pressure (gIMEP) is investigated at 1200 rpm with a single fuel injection per cycle. The fuel is n-heptane, selected for its low fluorescence compared to pump diesel fuel to avoid interference with the PAH-LIF and soot-LII signals. It also has essentially zero fuel-borne PAH, meaning all PAH in this study is combustion-generated. The ignition properties of n-heptane are similar to European diesel fuel, with a cetane number between 52.5 and 56 [14]. Different intake oxygen fractions were achieved by diluting the intake stream with nitrogen. An oxygen mole-fraction of 18% mimics typical current diesel combustion using exhaust aftertreatment [15], while 10.5% intake oxygen is low enough that exhaust aftertreatment for soot and nitrogen oxides (NOx) may not be required [15]. Additionally, the low combustion temperatures at 10.5% oxygen further slow PAH/soot kinetics so that their formation pathways can be studied in more detail.

2.2. Excitation setup

Two independent 10-Hz Spectra Physics Quanta Ray Nd:YAG laser systems provide the two excitation beams. One (model GCR-250) is used at its fundamental (1064 nm) for soot-LII. A second (PRO-200) excites PAH-LIF using either its second (532 nm) or fourth (266 nm) harmonics. Additionally, a Spectra-Physics optical parametric oscillator provides pulsed laser light at 633 nm.

One at a time, the 266/532/633-nm laser beams are combined with the 1064-nm beam and co-aligned with the approximate symmetry plane of one of the eight fuel jets, angled at 14° relative to the firedeck. The beams are formed into 30-mm wide sheets that are less than one mm thick over the region of interest with pulse energies of 50-60 mJ at 266 and 532 nm, 40 mJ at 633 nm, and 250 mJ at 1064 nm. The 1064-nm fluence exceeds 0.8 J/cm^2, which was found to be sufficient to reach a plateau in the LII signal strength such that a further increase in fluence does not significantly affect the LII signal.

2.3. Detector setup

As shown in Fig. 1, the soot-LII signal is directed by the 45-degree mirror and a 50-50 beam splitter to a Xybion gated, intensified CCD camera (model ISQ-350-W-3). The camera is equipped with SWP450 and GG385 filters and a 105-mm focal-length glass lens at f/4. As described in [16], laser-heated soot (LII) emits more strongly at shorter wavelengths than combustion-heated soot, so using a shorter spectral band from 385 to 450 nm improves the signal-to-noise ratio relative to combustion-heated soot. The laser pulse is bracketed with the minimum intensifier gate width of 60 ns.

The PAH-LIF signal is imaged by a PI-MAX3 ICCD camera with an HQf intensifier and another 105-mm glass lens at f/4. The intensifier gateoverlaps the laser pulse with the minimum achievable 2.47-ns width to maximize the signal-to-noise ratio. A short-wave-pass filter with a 50% cut-off near 850 nm (CVI/Melles-Griot FSWP-850) removes scattered 1064-nm light. Narrow-band notch filters and a WG285 color filter reject elastically scattered light at 532/633 and 266 nm, respectively.

In each engine run, 20 images are acquired at a fixed crank angle, with every fourth image capturing background luminosity without any laser light. The LII laser pulse trails the LIF pulse by 1 μs, which is sufficient to separate the two signals while being virtually simultaneous relative to engine time scales. The order of the two pulses did not affect the acquired images, as observed previously [10]. From each image set, a single representative image pair is objectively identified using a statistical image-correlation technique [17].

For spectral measurements, an Oriel 77250 monochromator is used as a spectrograph by mounting a Xybion intensified CCD camera (model ISG-250-UX-3) at the exit plane. A 300 lines/mm grating (Oriel #77939) resolves the 400 to 700 nm range with a spectral resolution of 8 nm at 500 nm. The entrance slit is lens-coupled to the probe volume using a 50-mm glass lens at f/4 (Fig. 1). Spectrograph images are acquired in sets of 20 at each crank angle. For laser-induced spectra, the minimum intensifier gate of 110 ns brackets the desired laser pulse, whereas for chemiluminescence spectra the gate is increased to 140 microseconds, or about 1°CA. The laser-induced spectra are background-luminosity-subtracted (removing very weak natural emission with the short gate), median-filtered, spatially binned over the head of the jet, and ensemble-averaged. The chemiluminescence spectra are only spatially- and ensemble-averaged. All spectra are made quantitative by correcting for the filter transmission and camera spectral sensitivity using a Hoffman calibrated integrating sphere, model LR-6Z.

Finally, a large-area (1 cm^2) photodiode viewing through the piston-crown window records the natural combustion-luminosity, with system sensitivity set to resolve the strong soot luminosity, but not the relatively weak chemiluminescence.

3. Results and discussion

Figure 2 shows image sets for 10.5% and 18% intake-oxygen, with 532-nm LIF and 1064-nm LII acquired virtually simultaneously in each image, but each image-pair at a different crank angle is from a different engine run. LIF and LII images are false-colored green and red, respectively, such that overlap regions appear yellow. Because of the possibility of soot LII in the signal from 532-nm (as well as 266 and 632-nm) excitation, overlap areas may or may not have PAH, but certainly have soot. The injector position and bowl-rim position are indicated in the images, with one of the eight fuel jets propagating horizontally left to right across the image.

Because of the different dynamic ranges of the cameras and to make initial soot-formation visible, both the LII and the LIF signal images are artificially amplified such that 0.1 percent of the pixels in the area of interest saturates. These post-processing gains, color-coded according to the false-color scheme, are displayed in each image. The left side of each image in Fig. 2 shows various degrees of scattering/interference from the 1064-nm beam (red). The scattering appears worse in the early images because of higher gains (as indicated on the images).

3.1. 532-nm LIF and 1064-nm soot LII imaging at 10.5% and 18% intake oxygen

The top of Fig. 2 shows the measured injection rate, the apparent rate of heat release (ROHR) and the soot-luminosity photodiode signal. Vertical dashed-lines indicate the crank angles of the images. The ROHR and soot luminosity show that ignition and soot-formation processes are slower at 10.5% intake oxygen than at 18% oxygen.

With 10.5% intake oxygen, 532-nm PAH-LIF (green) is first detected immediately after the premixed heat-release peak, near 370 CAD. Thereafter, the PAH-LIF area grows without any detectable soot-LII until 374 CAD, at which time the photodiode also detects soot natural luminosity (top). After this 4 °CA inception delay, soot-LII signal quickly fills the regions where PAH were present, yielding increasing signal on both cameras (note decreasing gains in later images).

Also for 10.5% intake oxygen, a conventional combusting diesel jet structure [16] is not apparent because of the long mixing time. Instead, the soot distribution is a consequence of jet/wall/swirl dynamics preceding soot formation. Prior to ignition and combustion, the jet impinges and spreads along the bowl wall. The counterclockwise swirl-flow sweeps the originally horizontal jet partially out of the laser sheet, while parts of the adjacent clockwise jet are transported into the bottom of the laser sheet. Hence, the large structure in the bottom of the images at the end of the sequence (378 CAD) is a remnant of the interaction between two adjacent jets.

For 18% intake oxygen (Fig. 2, right), a more conventional combusting diesel jet is apparent. Over the narrower crank-angle range of images (to 366 CAD) than at 10.5% oxygen (to 378 CAD), the jet is transported counterclockwise only slightly by swirl. PAH-LIF is again first detected immediately after the premixed burn (361 CAD). Within 1 °CA, the

PAH-LIF is typically surrounded by soot-LII. While some portions display pure PAH (green), the rapid increase in soot (note the decreasing 'red' gains) yields LII signal on both cameras. Soot luminosity is also much higher than at 10.5% intake oxygen (Fig. 2, top).

3.2. Multi-wavelength imaging comparison

LIF originating from 266, 532, and 633-nm excitation is compared at 10.5% intake oxygen fraction, where the evolution of PAH is slowest and thus most easily studied. Fig. 3 shows three time-sequences of representative composite images from LIF excitation at these three wavelengths (false-colored green) with simultaneous 1064-nm LII (false-colored red).

Comparing the left and middle sets of images in Fig. 3 shows that combustion-generated species, very likely PAH, can be detected earlier with 266-nm than with 532-nm excitation. The onset of fluorescence resulting from excitation at 266 nm occurs between 368 and 369 CAD. In the 370 and 371 CAD images, the signal for 266-nm excitation is stronger than for 532-nm excitation. Recall that the images use different gains as indicated on each image.

Excitation at 633 nm shows signal only at later crank angles, starting from 371 CAD. Furthermore, signal from 633-nm excitation, presumably fluorescence of very large PAH, arises before any LII. This implies that (very large) PAH can absorb light at the red HeNe-laser wavelength (~633 nm). While this to some extent may open possibilities for fluorescence detection of such species, absorption by very large PAH may also interfere with soot-extinction measurements that use HeNe lasers; the extinction will be increased beyond that caused by soot alone, especially near soot inception. At later crank angles when soot is more dense, absorption by PAH would likely become less significant, or even insignificant, relative to extinction by soot.

All three image sequences show a consistent PAH signal development. A temporal redshift in absorption (excitation) wavelength, and hence growth in PAH molecular size (i.e., number of rings), occurs over a short 3-4 °CA range. In the ensemble, no spatial differences are apparent among the different excitation-wavelength/size classes; when long-wavelength LIF is present, similar regions in images from different cycles show short-wavelength LIF.

Figure 3 shows that to detect the earliest (and smallest) PAH, 266-nm laser light is appropriate. However, laser-light as well as the corresponding emission are more readily attenuated at shorter wavelengths. While most of the window-deposited soot in the path of the laser is blasted away by laser pulses between skip-fired cycles, attenuation by the soot cloud itself [18] and soot deposits on the piston window can be problematic, especially at high-sooting conditions. Furthermore, components of commercially available fuels, as well as (intermediate) combustion products, may be excited by 266-nm laser light, thereby confounding the fluorescence signal. Hence, while 266-nm PAH-LIF can be useful for fuels/conditions such as those employed here, excitation of PAH-LIF at 532 nm has a broader utility.

3.3. Spectral analysis of LIF and LII at 10.5% intake oxygen

Figure 4 shows quantitative LIF and LII spectra for the 10.5% oxygen condition of Fig. 3. Spectral ranges where the filters have high absorbance are artificially masked for clarity. At 374 CAD, at which time the soot-LII (not shown) is relatively weak, the 532-nm LIF spectrum is broad, peaking near 550 nm (~5300-K blackbody), and without any narrow peaks attributable to small combustion intermediates such as CH or C_2. Shortly thereafter, at 376 CAD, the broad 532-nm LIF emission is more redshifted, peaking near 600 nm (~4800-K blackbody). The 1064-nm soot-LII spectrum at 376 CAD is similarly broad, but exhibiting an even more redshifted peak between 600 and 650 nm (~4600-K blackbody). As explained earlier, the emission from 532-nm excitation likely includes soot LII when soot is present, so the similarity to the soot-LII spectrum from 1064-nm excitation is not unexpected. At even later timings (not shown), the LIF spectra become even more similar to the soot-LII spectra, suggesting that the signal from 532-nm excitation becomes dominated by soot-LII.

The 266 and 633-nm LIF emissions are also spectrally resolved at the same two crank angles as for 532 nm. Considering 266-nm excitation first, at the early crank angle of 374 CAD, the LIF spectrum is much different than the LII signal, peaking at <450 nm (>6400-K blackbody), which is inconsistent with incandescence at the soot vaporization temperature (4000-4500 K). (The peak may actually lie in the ultraviolet, which is not resolved in these measurements.) Hence, emission from 266-nm excitation at this and earlier crank angles can be interpreted as being almost solely LIF, not having significant LII, consistent with the images in Fig. 3. At later crank angles, the signal likely contains more and more LII, resulting in a red-shift of the spectral peak.

The 633-nm induced LIF spectra are somewhat weaker than for 266 and 532-nm excitation (see Fig. 3), especially at 374 CAD. Nonetheless, the spectrum at 374 CAD displays proportionally more light red-shifted from the 633-nm excitation wavelength than those of the shorter wavelength excitations. At the later crank angle (376 CAD) the shape of the LII and 633-nm LIF spectra are so similar that no LIF signal can be distinguished from LII.

A significant portion of the early LIF emission (at 374 CAD) for both 532-nm and 633-nm excitation is blue-shifted from the laser wavelength. (A similar effect may occur for 266-nm, but is not resolved here). A similar blueshift was observed in a previous study with this same engine under conditions with no detectable 1064-nm soot LII signal [10]. The source of the blue-shifted emission is unclear, but one possible source is laser-excitation of PAH that are already in excited ro-vibrational states. PAH already in excited states can relax to lower ground states after electronic excitation by the laser light, thereby yielding blue-shifted emission. For large PAH molecules with so many ro-vibrational modes, much of the ground electronic state can be in higher ro-vibrational states for thermal distributions at combustion-heated temperatures. In addition, non-thermal ro-vibrational distributions resulting from combustion chemistry can increase the amount of

blue-shifted emission. Chemiluminescence spectroscopy described in the next section provides some support for the possibility of non-thermal ro-vibrational distributions.

3.4. Chemiluminescence spectroscopy

Figure 5 shows natural chemiluminescence emission spectra for the 10.5% oxygen condition, using a much longer (140 microsecond) camera gate than the PAH-LIF experiments (110 ns). The spectra span from first heat release to the last crank angle before soot-LII and soot luminosity appear. From the earliest crank angle, the emission spectrum is broadband, peaking in the blue. This early broadband emission spectrum is consistent with the CO_2* emission [19] spectrum, ranging from 340 to about 650 nm with its peak around 400 nm. Over the next few °CA, the broadband signal strength increases, especially at longer wavelengths. A slight hump is visible near 431 nm, corresponding to the excited CH* radical [20], and a distinct chemiluminescence peak near 590 nm may be from sodium impurities in the fuel, as sodium-doped flames have a strong isolated line near 589 nm [19].

The chemiluminescence spectrum departs from the initial CO_2* emission spectrum starting at 368 CAD, which is the same crank angle as the first detectable PAH-LIF in the images of Fig. 3 for 266-nm excitation (small PAH). After this initial rise in natural emission (potentially PAH chemiluminescence), its red-peaked broadband emission rises through the same crank-angle range in Fig. 3 where PAH-LIF signals arise with 532-nm (370 CAD) and then 633-nm (371 CAD) excitation. At later crank angles, the natural emission grows rapidly, especially after 374 CAD when soot luminosity and soot-LII become significant in Figs. 2 and 3, respectively. For clarity, the very bright spectra from these later crank angles are not shown here. As the soot luminosity signal eventually becomes orders of magnitude stronger than the chemiluminescence, any narrow spectral features disappear into a broad continuum whose spectral peak shifts further towards the infrared. However, the detection of significant PAH chemiluminescence (molecules in excited electronic states), make it reasonable to expect that also PAH molecules are in excited vibrational states, which could cause the PAH-LIF blue-shift in Fig. 4. Furthermore, the increased short-wavelength emission from PAH chemiluminescence would also explain the unreasonably high apparent soot temperatures observed near the onset of soot formation in two-color pyrometry measurements, especially for LTC conditions [21].

4. Conclusions

In an optically accessible diesel engine, imaging PAH-LIF from pulsed-laser excitation at 266, 532, and 633 nm reveals the temporal growth of PAH molecules, while soot-LII from a 1064-nm pulsed laser indicates inception to soot. At a LTC engine operating condition with 10.5% intake-oxygen, PAH is first detected by 266-nm excitation just after the premixed heat release peak, followed by 532-nm and then 633-nm excitation, indicating a likely temporal growth of PAH molecular size. The PAH-LIF region also grows spatially during the approximately 5-6 °CA before soot-LII is first detected. For 18% intake oxygen, first PAH are also detected just after the premixed burn, but within 1 °CA, the PAH region is surrounded by soot, though some images display regions of pure PAH.

The LIF signals have broadband spectra, much like LII, but typically with a blue-shifted peak, such that the LIF spectrum is spectrally inconsistent with laser-heated soot. A substantial portion of the LIF emission is at wavelengths shorter than the excitation laser, suggesting that many of the combustion-generated PAH are in excited ro-vibrational states. The LIF signal with 633-nm excitation is weaker than for 266 or 532-nm excitation, and more difficult to distinguish spectrally from LII because the broadband peaks are at similar wavelengths. Imaging comparisons with 1064-nm soot-LII show that 633-nm LIF does precede LII, however. At later crank angles, the contribution of LII grows to dominate the LIF signals, so that the emission is spectrally indistinguishable from LII.

Quantitative chemiluminescence spectroscopy also shows CH (430 nm) and sodium (590 nm) features on a broad emission spectrum, probably from PAH chemiluminescence, whose initial emergence temporally coincides with first detection of the 266-nm PAH-LIF. The existence electronically excited PAH yielding chemiluminescence is consistent with the hypothesis that the strong short-wavelength portion of the LIF emission spectrum is from ro-vibrationally excited PAH, and may also explain anomalously high apparent temperatures at soot inception in soot optical thermometry measurements. At later crank angles, a soot-luminosity signal appears, coinciding with the first soot-LII, and the narrow spectral features disappear as the LII quickly strengthens by orders of magnitude and the spectral peak shifts further toward the infrared.

The detection of apparent PAH-LIF from 633-nm excitation suggest that very large PAH absorb light at HeNe-laser wavelengths in a narrow crank-angle range prior to the formation of soot. While this to some extent may open possibilities for fluorescence detection of such species, absorption by large PAH may also interfere with soot extinction measurements that use HeNe lasers by increasing the extinction beyond that caused by soot alone, especially near soot inception. At later crank angles when soot is more dense, absorption by PAH would become less significant, or even insignificant, relative to extinction by soot.

Acknowledgements

Support for this research at the Combustion Research Facility, Sandia National Laboratories, Livermore, CA, was provided by the U.S. Department of Energy, Office of Vehicle Technologies. Sandia is a multi-program laboratory operated by Sandia Corporation, a Lockheed Martin Company for the United States Department of Energy's National Nuclear Security Administration under contract DE-AC04-94AL85000. Keith Penney and David Cicone are gratefully acknowledged for their assistance with experiments.

References

[1] M. Musculus, P. Miles, L. Pickett, Prog Energy Combust Sci 39 (2-3) (2013) 246-283.

[2] J. Warnatz, U. Maas, R. Dibble, Combustion, Springer, Berlin-Heidelberg, Germany, 2006.

[3] R.N. Westerholm, T.E. Alsberg, A.B. Fromelln, M.E. Strandell, U. Rannug, L. Winquist, V. Grigoriadis, K.-E. Egebäck, Environmental science & technology 22 (8) (1988) 925-930.

[4] D.W. Dockery, C. A. Pope, X. Xu, J. D. Spengler, J. H. Ware, M. E. Fay, B. G. Ferris, F. E. Speizer, N Engl J Med 329 (1993) 1753-1759.

[5] H. Bockhorn, Ed., Soot formation in combustion, Springer, Berlin-Heidelberg, 1994.

[6] T. Aizawa, H. Kosaka, Int J Engine Res 9 (2006) 79-96.

[7] K. Hayashida, K. Amagai, K. Satoh, M. Arai, J Eng Gas Turbines Power 128 (2006) 241-246.

[8] R. Rieger, K. Müllen, J Phys Org Chem 23 (2010) 315-325.

[9] R.L. Vander Wal, K.A. Jensen, M.Y. Choi, Combust Flame 109 (1997) 399-414.

[10] M.K. Bobba, M.P.B. Musculus, Combust Flame 159 (2012) 832-843.

[11] M. Musculus, L. Pickett, Combust Flame 141 (4) (2005) 371-391.

[12] J. O'Connor, M. Musculus, SAE Int J Engines 6 (1) (2013) 379-399 (2013-01-0910).

[13] J. O'Connor, M. Musculus, Int. J Eng Research (in press) (2013), doi:10.1177/1468087413488767 .

[14] M. Murphy, J. Taylor, R. McCormick, Compendium of experimental cetane number data, National Renewable Energy Laboratory, NREL/SR-540-36805, 2004.

[15] P. Brijesh, S. Sreedhara, Int J Automotive Technology 14 (2) (2003) 195-206.

[16] J.E. Dec, SAE Trans 106 (3) (1997) 1319-1348 (970873).

[17] C. Genzale, *Optimizing Combustion Chamber Design for Low-Temperature Diesel Combustion*, PhD thesis, University of Wisconsin-Madison, USA, 2008.

[18] M.Y. Choi, K.A. Jensen, Combust Flame 112 (4) (1998) 485-491.

[19] A.G. Gaydon, The spectroscopy of flames, Chapman and Hall, London, UK, 1974.

[20] Y. Hardalupas, M. Orain, Combust Flame 139 (3) (2004) 188-207.

[21] E. Huestis, P.A. Erickson, M.P.B. Musculus, SAE Trans 116 (4) (2007) 860-879 (2007-01-4017).

Table 1

Engine specifications and operating conditions

Compression Ratio	11.22:1
Common-rail injector	Cummins XPI
Nozzle hole arrangement	8×140 µm×14°
Fuel rail pressure	1000 bar
Command start of injection	352 CAD
Command injection duration	2.5 ms
TDC motored density	16.6 kg/m^3
TDC motored temperature	975 K
Intake pressure	177 kPa (abs)
Intake temperature	155 °C
(Simulated 16:1 intake pressure)	116 kPa (abs)
(Simulated EGR rates)	30 – 59 %
Air excess ratio	2.39 at 21% O_2

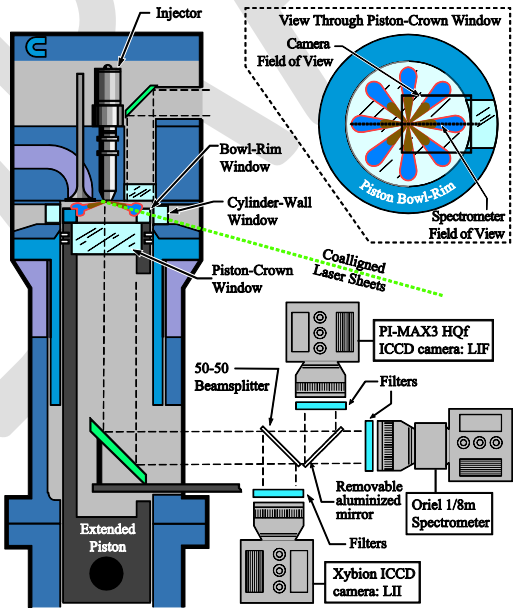

Fig. 1. Schematic of the single-cylinder engine, laser configuration, and optical detector system.

The camera and spectrometer field-of-view are shown in the upper right corner.

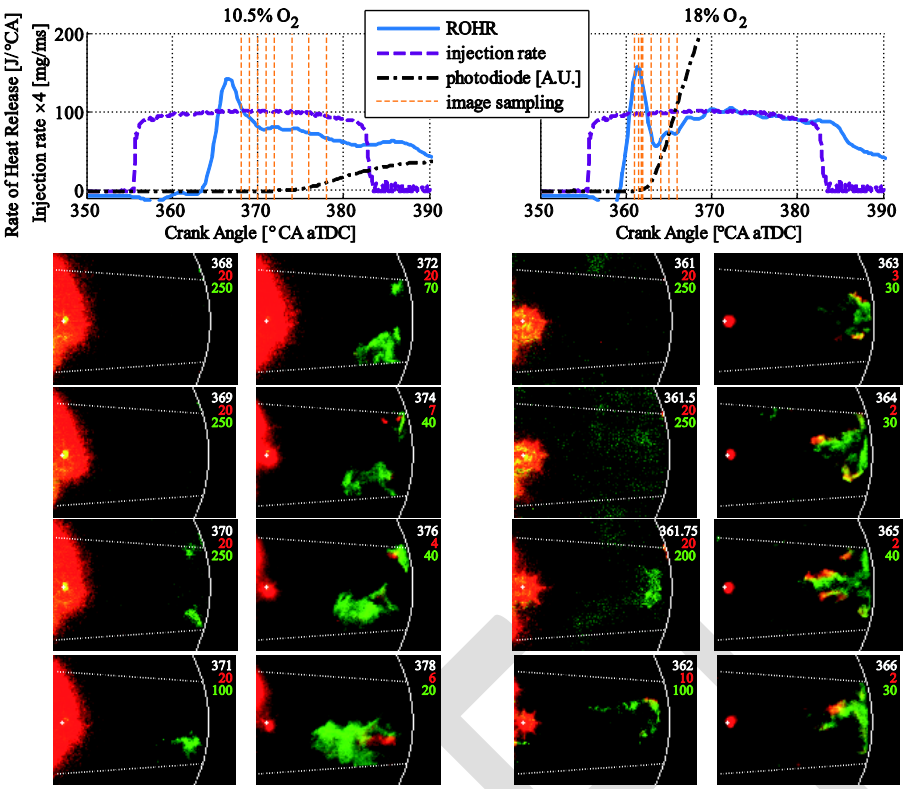

Fig. 2. Top: ROHR, injection rate and natural soot luminosity signals for 10.5% (left) and 18% (right) intake oxygen fractions. Bottom: composite single-shot images, false colored for 532-nm LIF (green) and LII (red) with image crank angle and color-coded signal gains are denoted in each image. (For interpretation of the references to color in this figure, the reader is referred to the electronic version of this paper.)

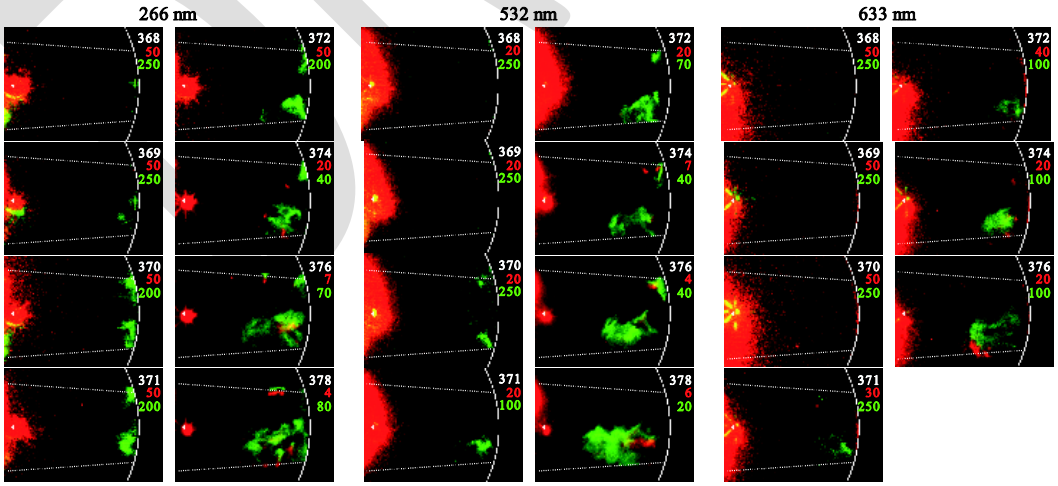

Fig. 3. Composite single-shot images, false-colored for LII excitation at 1064 nm (red) and LIF excitation (green) at 266, 532 or 633 nm, as indicated by the column titles. Operating conditions correspond to Fig. 2. (10.5% O_2). Image crank angle and color-coded signal gains are denoted in each image. (For interpretation of the references to color in this figure, the reader is referred to the electronic version of this paper.)

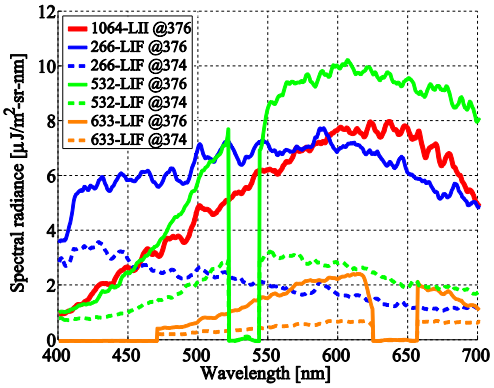

Fig. 4. Spectra of the laser-induced signal for excitation laser wavelengths of 266, 532 and 633 nm (labeled "LIF") and 1064 nm (labeled "LII") at 374 and 376 CAD. 10.5% intake oxygen condition (Fig. 3).

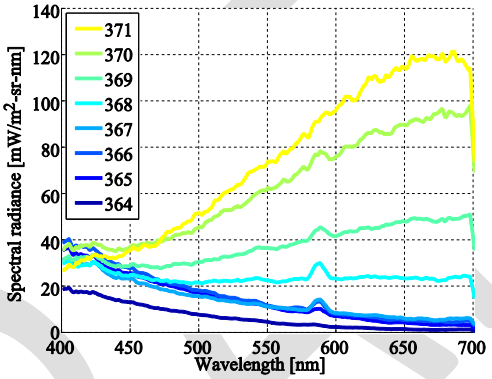

Fig. 5. Quantitative chemiluminescence emission spectra for an early crank angle range of the 10.5% intake oxygen condition (Fig. 2, left). Legend indicates the starting crank angle of the 1 °CA camera gate.